Aerodynamic simulation of evacuated tube maglev trains with different streamlined designs

Xuyong CHEN, Lifeng ZHAO[*], Jiaqing MA, Yuansen LIU

Key Laboratory of Magnetic Levitation Technologies and Maglev Trains (Ministry of Education of China), Superconductivity and New Energy R&D Center, Southwest Jiaotong University, Chengdu 610031, China

Abstract: Based on the Navier-Stokes (N-S) equations of incompressible viscous fluids and the standard k-ε turbulence model with assumptions of steady state and two dimensional conditions, a simulation of the aerodynamic drag on a maglev train in an evacuated tube was made with ANSYS/FLOTRAN software under different vacuum pressures, blockage ratios, and shapes of train head and tail. The pressure flow fields of the evacuated tube maglev train under different vacuum pressures were analyzed, and then compared under the same blockage ratio condition. The results show that the environmental pressure of 1 000 Pa in the tube is the best to achieve the effect of aerodynamic drag reduction, and there are no obvious differences in the aerodynamic drag reduction among different streamline head shapes. Overall, the blunt-shape tail and the blockage ratio of 0.25 are more efficient for drag reduction of the train at the tube pressure of 1 000 Pa.

Key words: aerodynamic drag; evacuated tube maglev train; blockage ratio; train head and tail

1. Introduction

The forthcoming energy shortage and the need to travel fast present many difficulties in the 21st century for traditional transportation, such as shipping, railway, waterway, and road transportation [1]. To solve these problems, Oster [2-3] proposed the concept of evacuated tube transportation (ETT). The ETT has numerous advantages such as high speed, low aerodynamic drag, low noise pollution, safety, less energy consumption, etc [4-6], and some solutions of the key vacuum technology for ETT have also been proposed [7].

Aerodynamics is a key issue for the application of evacuated tube maglev trains (ETMT) and therefore should be investigated thoroughly [8]. In recent years, several efforts of aerodynamic drag simulation were reported on a ETT train with a speed of 200 m/s and a tube pressure of above 1 000 Pa [9-10], and other efforts in numerical simulation of aerodynamic drag were reported on a subsonic ETT train with speed ranging from 50 to 300 m/s and tube pressure from 10 to 10 000 Pa [11]. Kwon et al. [12] concluded that the aerodynamic aspects must be included in the optimal design of the train nose, which is an improvement over

current design in terms of micropressure wave [13]. Streamline design of train head or tail and the related research has been conducted for traditional high-speed trains [14-16], metro trains [17], and maglev trains [18-19]. However, little research has been done on the head and tail optimization of the ETMT.

In the present work, the external flow field of the maglev train with a speed of 300 m/s in an evacuated tube was simulated with ANSYS/FLOTRAN software, based on the viscous fluid mechanics theory and the two-dimensional incompressible viscous flow model. By considering different vacuum environments, three head types, and five tail types of trains for 0.11, 0.14, 0.18, 0.25, and 0.36 blockage ratios, we studied the relationships between the aerodynamic drag, shape of head and tail, and blockage ratio of the train. The results obtained may provide a helpful reference for future ETMT applications.

2. Numerical model

2.1. Basic assumptions

(1) The ETMT is assumed to run at a speed of 300 m/s with a Mach number of 0.88. As the Reynolds number of the flow field is greater than 10^5, the flow field is considered turbulent, and the k-ε two-equation turbulence model is used to simulate the flow field.

(2) The tube pressure of most models are assumed to be 1 000 Pa. Considering the computation time, conver-

gence degree, computer performance, and blockage ratio, the gas is assumed to be incompressible. The tube temperature is assumed to be 293 K.

(3) The simulation in this paper is dealt with in two dimensions. The largest longitudinal section of the maglev train is selected as the calculation plane, and the connection of the whole maglev train is assumed smooth.

(4) As the magnetic resistance is assumed to be negligible, only the aerodynamic drag is considered. According to the formula of aerodynamic drag, $F=\Delta PS$, the relationship between the aerodynamic drag F and the pressure difference ΔP between the head and tail of the ETMT is linear, considering the largest cross-section area S of the maglev train constant. Throughout this paper, the pressure difference ΔP means the difference between the maximum and minimum pressure values within the longitudinal scope of the train body from head to tail.

2.2. Mathematical model

The standard k-ε turbulence model of the two-dimensional viscous, steady and incompressible turbulent flow field is adopted to simulate the flow field of the ETMT. The control equations of the flow field mathematical model are as follows [20]:

continuity equation:

$$\nabla \cdot U = 0; \tag{1}$$

conservation equations of momentum:

$$\nabla \cdot \left(\rho u U \right) = \nabla \cdot \left(\mu \nabla u \right) - \frac{\partial p}{\partial x}, \tag{2}$$

$$\nabla \cdot \left(\rho v U \right) = \nabla \cdot \left(\mu \nabla v \right) - \frac{\partial p}{\partial y}; \tag{3}$$

turbulent kinetic energy equation:

$$\nabla \cdot \left(\rho \kappa U \right) = \frac{\partial}{\partial y} \left[\left(\mu_1 + \frac{\mu_t}{\sigma_k} \right) \frac{\partial \kappa}{\partial y} \right] + \\ \mu_t \left(\frac{\partial u}{\partial y} + \frac{\partial v}{\partial x} \right) \frac{\partial v}{\partial x} - \rho \varepsilon; \tag{4}$$

dissipation rate of turbulent kinetic energy equation:

$$\nabla \cdot \left(\rho \varepsilon U \right) = \frac{\partial}{\partial y} \left[\left(\mu_1 + \frac{\mu_t}{\sigma_\varepsilon} \right) \frac{\partial \varepsilon}{\partial y} \right] + \\ \frac{\varepsilon}{\kappa} C_1 \mu_t \frac{\partial v}{\partial x} \left(\frac{\partial u}{\partial y} + \frac{\partial v}{\partial x} \right) - C_2 \rho \frac{\varepsilon^2}{\kappa}; \tag{5}$$

where U is the flow field velocity vector, in m·s^{-1}, u and v are the x and y components of U, respectively; p is the pressure of the flow field, in Pa; ρ is the air density, in kg·m^{-3}; μ_1 is the viscosity coefficient of laminar flow, in N·s·m^{-2}; k is the turbulent kinetic energy, in J·kg^{-1}; ε is the dissipation rate of the turbulence, in J·kg^{-1}; and, the parameter μ_t is given by $\mu_t=\rho C_\mu k^2/\varepsilon$, where C_1=1.47, C_2=1.92, C_μ=0.09, σ_k=1.0, and σ_ε=1.3.

2.3. Longitudinal profile models of the maglev train

In this research, different longitudinal profiles are designed for the ETMT, including three types of train heads and five types of tails, as shown in Fig. 1 and Fig. 2.

The basic parameters of the ETMT compartment are set as length 35 m and height 3 m. The length of the rear and front portion will vary with the design style. For example, the entire train length is 41 m when it has a semicircle tail and a head with a radius of 3 m, as shown in Fig. 3. Different streamlined designs of the tail also cause the train length to change (Fig. 2).
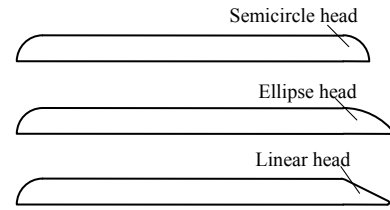

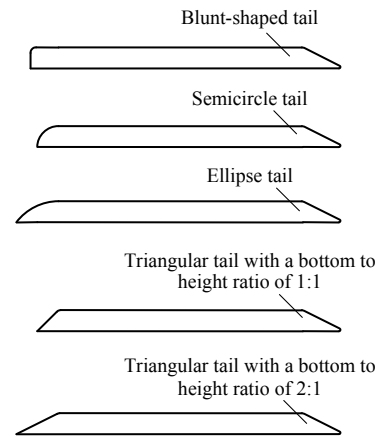Fig. 1 Different models of ETMT head
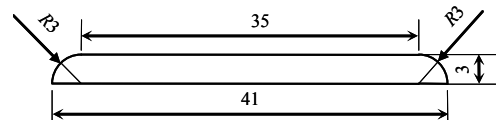

Fig. 2 Different models of ETMT tail

Fig. 3 Dimensions of the model train (unit: m)

2.4. Simulation scenarios

We developed simulations for three situations. The first is to analyze the influence of pressure on the ETMT under different vacuums. The second is to analyze three types of heads (Fig. 1) for the ETMT running under different blockage ratios. The third is to analyze the five types of tails (Fig. 2) for the ETMT running under a specific blocking ratio. Moreover, pressure differences of the blunt-shaped tail and the semicircle tail in different blocking ratios are compared according to the calculation results. For the second and third situations, the tube pressure is set as 1 000 Pa, and the ETMT speed is 300 m/s.

Using the ANSYS/FLOTRAN software, the flow pressure fields are simulated based on Eqs. (1) to (5) for the ETMT with different combinations of heads and tails, and the nephograms of ETMT in various situations are generated.

2.5. Computational domain

For the blockage ratios of 0.11, 0.14, 0.18, 0.25, and 0.36, the tube diameter is set to be 9, 8, 7, 6 and 5 m, respectively. One of the computational domain models is shown as an example in Fig. 4.

In Fig. 4, the entire tube length is 160 m and tube diameter (6 m, in this example) is set as the vertical height of the flow field. The total length of the ETMT chamber is 35 m, the distance from the rear boundary of the train chamber to the inlet of the evacuated tube is 47 m, and the distance from the front boundary of the train chamber to the outlet of the tube is 78 m.

2.6. Computing grid

With the movement of the maglev train, moving

meshing is used to deal with the constant change of the computational domain. The entire flow field area is divided into different sub-regions and separate meshes. The grids of various analytical model surfaces have a high density to ensure boundary layer calculation accuracy. The grids in the parts far away from the ETMT body, however, are not compacted in order to reduce the computation intensity and speed up convergence. For the situation shown in Fig. 4, a two-dimensional meshing model is given in Fig. 5.

3. Results and discussion

Taking points of the pressure nephograms on the ETMT surface sequentially from tail to roof and then to head, we obtained pressure curves as shown in Figs. 6, 7, and 13. Figs. 8 to 12 illustrate the pressure nephograms of the ETMT with the five types of tails (Fig. 2), running under a specific blocking ratio.

3.1. Pressure difference under different vacuums

Fig. 6 shows the pressure difference under different vacuums of the train with semicircle tail and linear head (Fig. 4). We can see that the effect of drag reduction on the maglev train is negligible when the vacuum pressure is less than 1 000 Pa. As the vacuum pressure increases from 1 000 to 10 000 Pa, the drag reduction effect enhances slowly, and then increases rapidly beyond 10 000 Pa. Thus the vacuum pressure of 1 000 Pa seems the best for ETT operation.

3.2. Pressure difference curves for different train heads

Fig. 7 shows the maximum pressure difference curves of the ETMT with different heads (Fig. 1) running in blockage ratios of 0.11, 0.14, 0.18, 0.25, and 0.36.
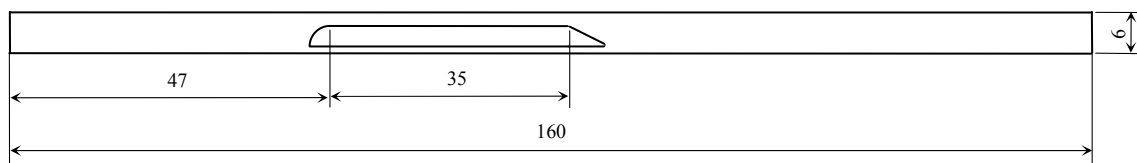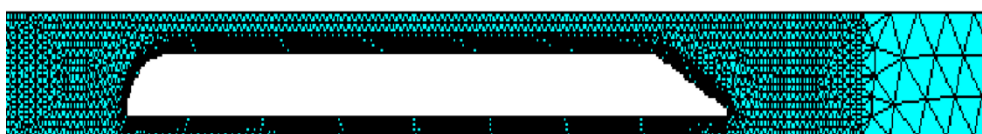

Fig. 4 Computational domain (unit: m)

Fig. 5 Partial view of the meshing

According to Fig. 7, the pressure differences for all head types increase with the blockage ratio. Furthermore, with the increase of blockage ratio, pressure difference increases slowly when the blockage ratio is less than 0.18, and then increases sharply beyond the blockage ratio 0.18. Meanwhile, we also notice that the pressure difference of the linear head is the smallest among the three head types, although their distinction is subtle.

Therefore, the drag reduction effect of the linear head is the best, and should be considered in the future application of the ETMT. In addition, the blockage ratio of 0.25 is more efficient at the tube pressure of 1 000 Pa.

3.3 Pressure fields of different tails

According to the results obtained above, we choose the linear head and a blockage ratio of 0.25 (tube diameter of 6 m) to examine the effects of different tails on the pressure difference, while the other parameters remain unchanged. The calculated results are shown in Fig. 8 to Fig. 12.
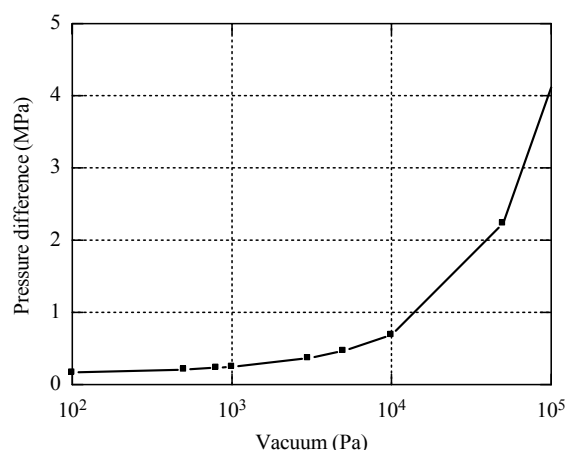

Fig. 6 Pressure difference under different vacuums
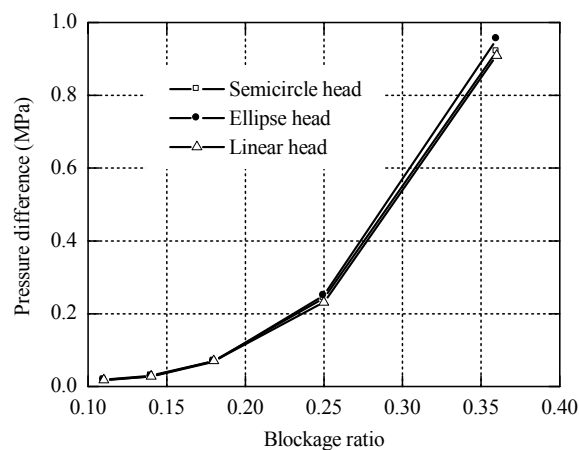

Fig. 7 Pressure difference vs. blockage ratio for different heads
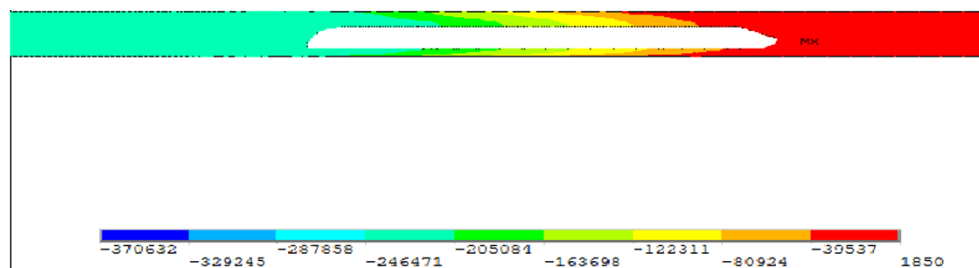

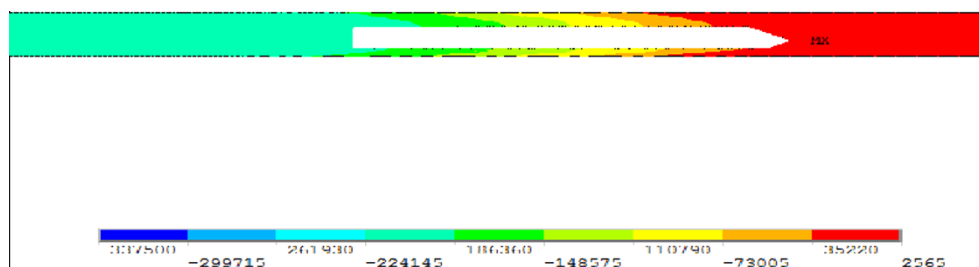Fig. 8 Pressure field of the train with a semicircle tail

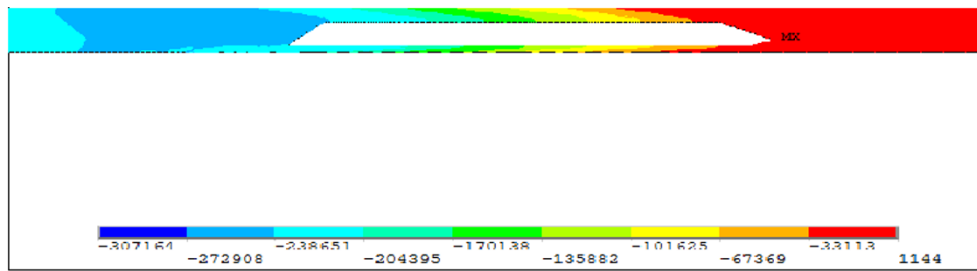Fig. 9 Pressure field of the train with a blunt-shaped tail

Fig. 10 Pressure field of the train with a triangular tail of 1:1 bottom to height ratio
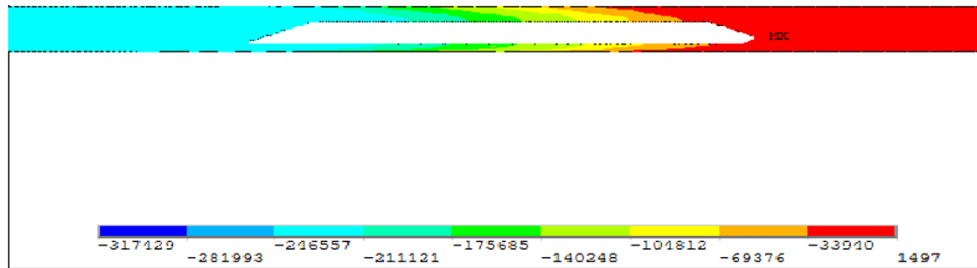

Fig. 11 Pressure field of the train with a triangular tail of 2:1 bottom to height ratio
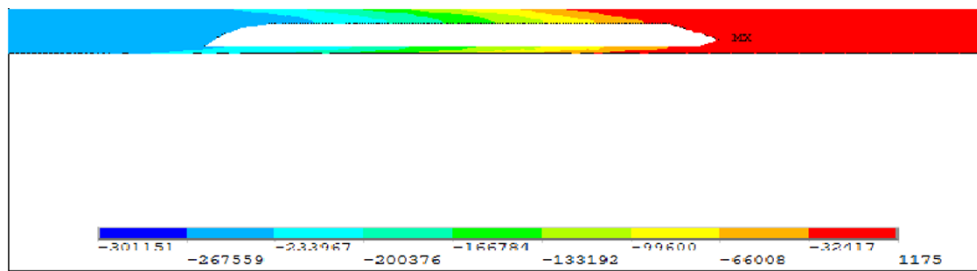

Fig. 12 Pressure field of the train with an ellipse tail

Table 1 Pressure difference ΔP with different tail shapes under the same blockage ratio of 0.25

Rear shape	ΔP (kPa)
Semicircle tail	237.3
Blunt-shaped tail	204.8
Triangular tail with a bottom to height ratio of 1:1	231.3
Triangular tail with a bottom to height ratio of 2:1	244.5
Ellipse tail	241.3

Fig. 13 Pressure difference vs. blockage ratio for semicircle tail train and blunt-shaped tail train

According to the pressure nephograms shown in Figs. 8 to 12, the pressure distributions for the different tails are similar. A high pressure region, where the highest pressure point is marked with MX in each figure, can be observed on the surface of the train head. The pressure decreases gradually along the longitudinal direction of the maglev train, and even turns negative. We also find that among the five types of tails, the train with the blunt tail possesses the maximum pressure
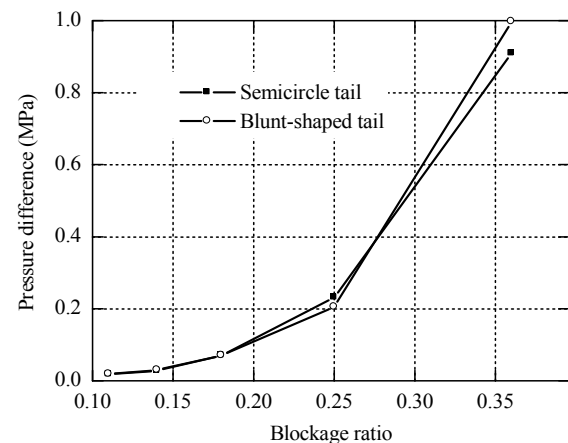
(2 565 Pa) on its head, while the pressure on the train head with a 1:1 bottom-height ratio triangular tail has the minimum value (1 144 Pa). This means that the pressure value on the head is affected by the tail shape.

Fig. 13 shows the curves of the maximum pressure difference between head and tail varying with blockage

ratio for linear head trains with blunt-shaped tail and semicircle tail. Pressure differences ΔP of the train with different tails is listed in Table 1. It is observed that the pressure difference of the maglev train with blunt-shape tail is apparently lower than others under the blockage ratio of 0.25. However, under the blockage ratio of 0.36, the pressure difference ΔP of the train with the blunt-shape tail is greater than that with the semicircle tail, as shown in Fig. 13. This reflects that the blockage ratio is also an important factor affecting the pressure difference value.

4. Conclusions

(1) The vacuum pressure plays a key role in the running drag of the ETMT. With the increase of vacuum pressure, the effect of the drag reduction increases very slowly when the pressure is less than 1 000 Pa, but rapidly when the pressure is above 10 000 Pa.

(2) The head with different streamlined designs does not cause obvious difference of aerodynamic drag effects for the maglev train running in the evacuated tube, but the linear head design can be regarded as one of the possible directions to reduce the aerodynamic drag of the ETMT in the future.

(3) The shape of tail exerts effects on the flow field around the train, causing the pressure on the train head and hence the pressure difference between head and tail to change, and this effect is also affected by blockage ratio.

Acknowledgments

References

[1] Y.P. Zhang, S.Z. Mei, X.G. Zeng, ETT-lead the high-speed transportation of the 21st century, *World Sci-Tech Research and Development*, 2002, **24**(2): 60-64.

[2] D. Oster, ET3, http://www.et3.com, 2004-05-12.

[3] D. Oster, Crystal River, Fla. Evacuated Tube Transportation, United States Patent: 5950543, 1999.

[4] D. Oster, M. Kumada, Y.P. Zhang, Evacuated tube transport technologies (ET3)[tm]: a maximum value global

transportation network for passengers and cargo, *Journal of Modern Transportation*, 2011, **19**(3):42-50.

[5] Y.P. Zhang, Y.Y. Li, Role and position of ETT in the future comprehensive transportation system, In: *The Proceedings of International Conference on Transportation Engineering 2007*, Chengdu, China, 2007: 2796-2803.

[6] Q.H. Qian, Some issues on design of underground magnetic levitation transportation system, *Tunnel Construction*, 2011, **31**(2): 155-160 (in Chinese).

[7] Y.P. Zhang, D. Oster, M. Kumada, et al., Key vacuum technologies to be solved in evacuated tube transportation, *Journal of Modern Transportation*, 2011, **19**(2): 110-113.

[8] Z.Y. Shen, On developing high-speed evacuated tube transportation in China, *Journal of Southwest Jiaotong University*, 2005, **40**(2): 133-137 (in Chinese).

[9] X. Zhou, Y.P. Zhang, Y.F. Yao, Numerical simulation on the aerodynamic drag of high-speed train in evacuated tube, *Science Technology and Engineering*, 2008, **28**(6): 1671-1819 (in Chinese).

[10] X. Zhou, D.Y. Zhang, Y.P. Zhang, Numerical simulation of blockage rate and aerodynamic drag of high-speed train in evacuated tube transportation, *Chinese Journal of Vacuum Science and Technology*, 2008, **28**(6): 535-538 (in Chinese).

[11] Y.P. Zhang, Numerical simulation and analysis of aerodynamic drag on a subsonic train in evacuated tube transportation, *Journal of Modern Transportation*, 2012, **20**(1): 42-50.

[12] H.B. Kwon, K.H. Jang, Y.S. Kim, et al., Nose shape optimization of high-speed train for minimization of tunnel sonic boom, *JSME International Journal Series C Mechanical Systems, Machine Elements and Manufacturing*, 2001, **44**(3): 890-899.

[13] J.S. Lee, J.H. Kim, Approximate optimization of high-speed train nose shape for reducing micropressure wave, *Structural and Multidisciplinary Optimization*, 2008, **35**(1): 79-87.

[14] J. Zhang, Research on optimum nose and tail shapes of foreign high-speed trains, *Electric Drive for Locomotive*, 2000, **35**(2): 16-18 (in Chinese).

[15] R.L. Chen, Q.Y. Zeng, J. Xiang, et al., Study on the performance of aerodynamics of high-speed train with different nose shapes, *Journal of Hunan University of Science and Technology (Natural Science Edition)*, 2009, **24**(1): 45-48 (in Chinese).

[16] Y. Yan, W.N. Fang, Analysis of head shape design of high-speed train, In: *Proceedings of the 2006 International Conference on Industrial Design and the 11th China Industrial Design Annual Meeting*, Hangzhou, 2006: 152-156 (in Chinese).

[17] J.R. Zhang, L. Zhou, Q.H. Sun, et al., Simulated calculation of distributing of air flow around metro train head and its design analysis, *Railway Locomotive and Car*, 2008, **28**(2): 43-47 (in Chinese).

[18] H.Q. Tian, D. Zhou, P. Xu, Aerodynamic performance and streamlined head shape of train, *China Railway Science*, 2006, **27**(3): 47-55 (in Chinese).

[19] S.G. Yao, P. Xu, Aerodynamic shape optimization of domestic maglev train, *Railway Locomotive and Car*, 2007, **27**(3): 33-34, 69 (in Chinese).

[20] H.Q. Tian, *Train Aerodynamics*, Beijing: China Railway Publishing House, 2007: 28-32 (in Chinese).

(Editor: Junsi LAN)